PERGAMON

International Journal of Heat and Mass Transfer 41 (1998) 4063–4080

International Journal of HEAT and MASS TRANSFER

Two- and three-dimensional numerical models of flow and heat transfer over louvred fin arrays in compact heat exchangers

K. N. Atkinson[a,*], R. Drakulic[a], M. R. Heikal[a], T. A. Cowell[b]

[a] *Department of Mechanical and Manufacturing Engineering, University of Brighton, Cockcroft Building, Moulsecoomb, Brighton BN2 4GJ, U.K.*

[b] *Delphi Automotive Systems European Technical Centre, GM Luxembourg, L-4940 Bascharage, G-D Luxembourg*

Received 5 November 1997; in final form 9 April 1998

Abstract

This paper presents a detailed evaluation of two- and three-dimensional numerical models of flow and heat transfer over louvred fin arrays in compact heat exchangers. Two 3-D models are described, both of which incorporate the effects of tube surface area and fin resistance on the overall heat transfer rate. Both of these features lead to a lowering of the predicted heat transfer rate per unit area compared with the 2-D model and, as a result, the 3-D models give predictions of overall heat transfer in better agreement with experimental observations. All of the models give accurate predictions of pressure losses, but it is argued that the superior heat transfer predictions of the 3-D models make them much more useful as design tools than 2-D models, even though they require much greater computing resources

Nomenclature

A_a heat transfer area
A_c minimum flow area
c_p specific heat at constant pressure
D_h hydraulic diameter
f overall friction factor
F_p fin pitch
G mass velocity ($=\rho U$)
h specific enthalpy
h_c heat transfer coefficient
k thermal conductivity
L fin length
L_p louvre pitch
$LMTD$ logarithmic mean temperature difference
m mass flow rate
Nu local Nusselt number
p pressure
Q heat flux
R specific gas constant for air
Re_{Dh} Reynolds number based on hydraulic diameter
Re_{Lp} Reynolds number based on louvre pitch
St overall Stanton number
t fin thickness
T absolute temperature of air
$T_{a,i}$ air temperature upstream of fin
$T_{a,o}$ air temperature downstream of fin
T_f absolute temperature of fin
T_p tube pitch
T_w tube width
u, v, w velocity components in x, y and z coordinate directions, respectively
U mean velocity through minimum flow area
x, y, z Cartesian coordinates.

Greek symbols
ΔT_i temperature difference $T_f - T_{a,i}$
ΔT_o temperature difference $T_f - T_{a,o}$
λ second coefficient of viscosity ($= -2/3\ \mu$)
μ dynamic viscosity of air
θ louvre angle
ρ air density
σ_{ij} viscous stress.

1. Introduction

Louvred plate fins are frequently used on the air side of automotive radiators and other heat exchangers to

* Corresponding author.

0017–9310/98 $19.00
PII: S0017-9310(98)00165-3

enhance the overall heat transfer rate. The louvres act to interrupt the air flow and create a series of thin boundary layers which have lower thermal resistance than the thick boundary layers on plain fins. Figure 1 shows a detail of a typical compact heat exchanger with flat-sided tubes and louvred plate fins.

Experimental studies aimed at optimising louvred fin geometries tend to be costly and time-consuming because of the large number of geometrical parameters involved (e.g. louvre angle, louvre length, fin length, fin pitch, no. of louvres—see Fig. 1). Only a few systematic experimental studies have appeared in the literature, the most comprehensive being those of Davenport [1, 2] and Achaichia and Cowell [3]. Although a number of automotive companies and heat exchanger manufacturers are known to have carried out experimental studies of louvred fin heat exchangers, very little of the experimental data has been presented in public, presumably because of the data's commercial value.

In the mid-1980s some of the first attempts were made to create 2-D numerical models of flow and heat transfer over louvred fin arrays using the techniques of computational fluid dynamics (CFD). At this time 3-D models were unfeasible because of their excessive computing requirements. Some of the first workers based their models on the assumption of zero fin thickness (e.g. Kajino and Hiramatsu [4]), while others made use of the fact that the flow eventually becomes periodic, and created models which compute the flow over only one louvre [5]. These limitations were due essentially to a lack of computing power and to a lack of CFD software and meshing capabilities for computing flows in complex geometries.

The object of this paper is to present a detailed evaluation of some recent flow and heat transfer computations for louvred fin arrays obtained with 2- and 3-D numerical models. The computations were made using a state-of-the-art CFD package (Star-CD) running on a powerful computer workstation (S.G.I. R10000 Solid Impact). Highly versatile mesh generation software was developed

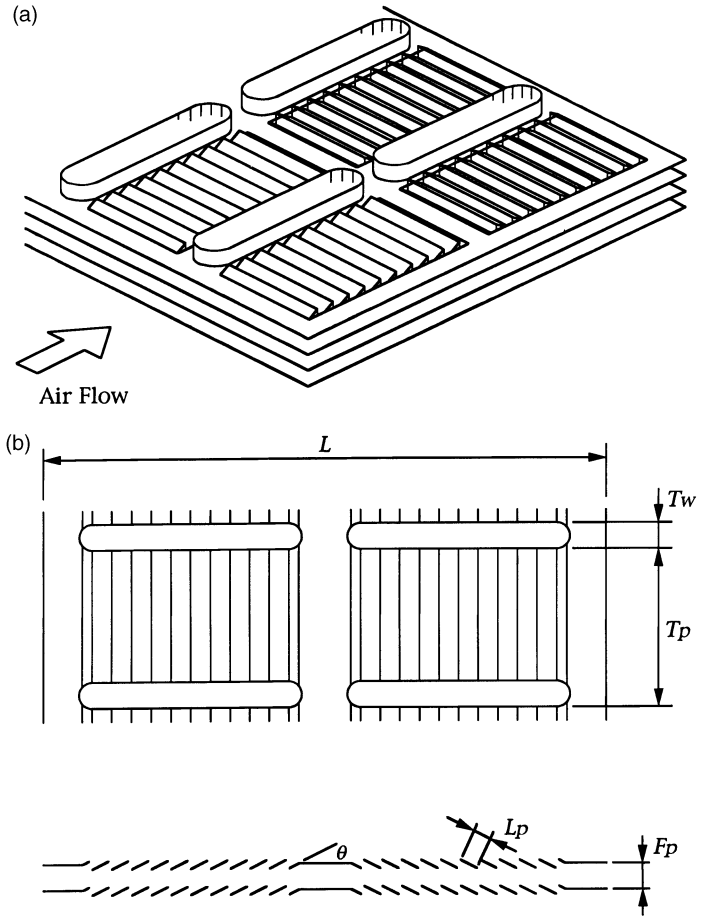

Fig. 1. Flat-tube and louvred plate fin heat exchanger. (a) Detail of heat exchanger. (b) Plan and side views of louvred fins and definitions of geometric parameters.

which was capable of creating numerical meshes for most fin geometries of practical interest. The meshes had a block structure with mainly rectangular cells for maximum numerical accuracy. Two 3-D models were created, both of which accounted for the effects of tube surface area and fin resistance on the overall heat transfer rate. It is shown that both of these features lead to a significant lowering of the predicted heat transfer rate per unit area, and are therefore essential components in the correct modelling of louvred-fin flows. Finally, to evaluate the models, computed values of overall Stanton number and friction factor were obtained for different Reynolds numbers and fin geometries and compared with measured values obtained on practical louvred fin heat exchangers by Achaichia and Cowell [3].

2. Literature review

Experiments on louvred fins can be divided into studies on actual-size fins and studies on large-scale models. The former tend to be concerned with the acquisition of design data such as overall friction factor and Stanton number, whereas the latter tend to be concerned more with understanding the detailed flow mechanisms which lead to heat transfer enhancement. The first person to conduct an experiment on a large-scale model appears to be Beauvais [6]. He presents a single photograph of a smoke trace in a ten-times scale model which clearly illustrates how the flow is redirected by the louvres. Up to that time it had been speculated that the louvres simply acted as roughness elements, with the flow being directed horizontally over the fin.

Wong and Smith [7] appear to be the first to demonstrate the validity of using large-scale models to simulate the flow over actual-size fins. They measured the overall drag coefficient and Nusselt number for a five-times scale model and found that the values agreed with those for an actual-size heat exchanger operating at the same Reynolds number.

Davenport [1] carried out smoke trace studies on a ten-times scale model of a non-standard variant of the corrugated louvred fin (the Z fin) and demonstrated that the degree of alignment between the flow and the louvres is a function of Reynolds number. At low Reynolds number the flow is mainly in the direction of the fin, whereas at high Reynolds number the flow is almost completely aligned with the louvres. Davenport conjectured that the change in alignment was due to the change in boundary layer thickness on the fin.

Davenport also carried out measurements of overall friction factor and Stanton number on actual-size louvred fin heat exchangers (Davenport [1, 2]). He found that when the friction factor and Stanton number were plotted against Reynolds number on log–log axes, the data had roughly constant slope of $-1/2$, consistent with the idea of a series of laminar boundary layers. At low Reynolds number he noticed a flattening of the Stanton number data, and conjectured that this was due to the change in flow alignment.

Achaichia and Cowell [3] made a comprehensive study of the performance characteristics of flat-sided tube and louvred plate fin heat exchangers. Their performance data encompass variations in all of the important geometrical parameters, including fin pitch, louvre pitch, louvre angle and tube pitch. Like Davenport, they found their data could be correlated more easily when the Reynolds number was expressed in terms of the louvre pitch rather than the hydraulic diameter of the air passages, again consistent with the idea of a series of laminar boundary layers. Achaichia and Cowell also noticed a flattening of the Stanton number at low Reynolds number and, like Davenport, they attributed it to the change in flow alignment.

The studies of Davenport [1, 2] and Achaichia and Cowell [3] represent the only major published sources of flow and heat transfer data on actual-size fins. There are a far greater number of studies in the literature on large-scale models aimed at investigating the flow mechanisms. Kajino and Hiramatsu [4] and Webb and Trauger [8], for example, use the dye-line flow visualisation technique to investigate the relationship between the flow alignment and the geometrical parameters louvre angle, louvre pitch and fin pitch. The dye-line technique also serves to indicate the conditions under which flow unsteadiness can occur. The study of Kajino and Hiramatsu [4], for example, shows that the flow remains essentially laminar and steady for Re_{Lp} up to about 1000. Antoniou et al. [9] present hot-wire measurements of mean velocity and r.m.s. velocity fluctuation in a 16-times scale model, and again show that the flow remains laminar and steady for Re_{Lp} up to about 1000. For $Re_{Lp} > 1000$, they detected velocity fluctuations downstream of the first one or two louvres in each bank, which they attributed to vortex shedding. Since practical fins usually contain a large number of louvres (20 or more in the fins studied by Achaichia and Cowell), these regions of unsteadiness constitute only a small fraction of the entire flow. Based on these experimental observations, most workers who have developed CFD models have tended to assume that the flow is entirely laminar and steady. For automotive applications, in which the Reynolds number ranges from about 200 to 1200, this assumption appears reasonable.

Baldwin et al. [10] and Kajino and Hiramatsu [4] were amongst the first workers to publish details of a 2-D numerical model of flow over louvred fins. In both models a rectangular solution domain was defined around the fin and the domain was divided into rectangular cells. In the model of Kajino and Hiramatsu the fin was assumed to have zero thickness, whereas in the model of Baldwin et al. the fin had finite thickness and was represented by defining some cells as solid regions. This gave the surface

of the louvres the appearance of a series of steps. Both models were evaluated using the results of studies on large-scale flow models. Baldwin et al. presented computations for two geometries with one Reynolds number each, corresponding to the LDA studies of Button et al. [11] and the hydrogen bubble visualisation studies of Hiramatsu and Ota [12]. The computations were found to display the same basic flow phenomena as in the experiments; in particular, it was found that flow alignment took longer to occur in the second louvre bank than in the first bank, agreeing with the smoke visualisation studies of Davenport [1]. Kajino and Hiramatsu [4] presented computed results for one geometry and one Reynolds number. They found that their computed streamlines agreed closely with the results of their own dye-line visualisation studies, and that their computed velocity profiles agreed well with their own velocity profiles deduced from hydrogen bubble studies. Kajino and Hiramatsu calculated the overall Nusselt number for the fin, but in neither of the two studies were computed values of overall pressure loss and heat transfer compared with measurements.

Achiachia and Cowell [5] computed the flow over a single zero-thickness louvre by employing a rectangular flow domain with uniform rectangular cells and with boundary conditions appropriate to periodic flow. They found that the degree of flow alignment increased with Reynolds number as observed in the experiments of Davenport [1], and they again attributed this to the change in boundary layer thickness. The authors carried out computations for a range of different geometrical parameter values and Reynolds numbers. As in the experiments of Kajino and Hiramatsu [4] and Webb and Trauger [8], for example, they found that the degree of flow alignment at a given Reynolds number increased as the fin-to-louvre pitch ratio was reduced. Achiachia and Cowell [5] did not compute the heat transfer from the fin, and although they presented computations of overall friction factor for the louvre, they did not compare these with any measured values.

Suga et al. [13] and Suga and Aoki [14] used a rectangular flow domain filled with overlapping Cartesian meshes to compute the flow and heat transfer over a finite-thickness fin. The Cartesian meshes were arranged so that mesh lines coincided with the fin surface. In the overlap regions values of variables were transferred from one mesh to another by bilinear interpolation. Suga et al. [13] compared computed velocity profiles for one geometry and Reynolds number with LDA measurements in a ten-times scale model and found reasonably close agreement. Also, for two Reynolds numbers, they compared values of Nusselt number averaged over each louvre with measurements for an actual-size fin obtained by uniformly heating each louvre using a nickel-film technique. In this case very close agreement was found. Suga and Aoki [14] carried out a computational study of the effect of louvre angle, fin pitch and fin thickness on overall heat transfer performance and pressure drop. Amongst their findings, they observed that the overall Nusselt number reaches a peak when the thermal wake downstream of each louvre passes down the middle of the gap between the louvres downstream, presumably because this maintains the greatest temperature difference between the air and the louvres. The authors presented values of overall Nusselt number and pressure drop for a wide range of parameter values and Reynolds numbers, but, as in other studies, they did not compare these with any measurements on practical heat exchangers.

In the 1990s several workers developed CFD codes based on non-orthogonal, boundary-fitted meshes to compute the flow over louvred fins [15, 16]. Other workers used non-orthogonal meshes in conjunction with commercial CFD codes [17, 18]. Hiramatsu et al. [15] for example, used a block-structured mesh with individual blocks for each louvre, whereas Achaichia et al. [17] used a novel mesh structure with mesh lines running parallel to the louvres and extending over several fins. Hiramatsu et al. [15] compared computed values of overall Nusselt number for one geometry and several Reynolds numbers with measurements for a uniformly heated fin by Shinagawa et al. [19] and found close agreement. They also compared values of computed and measured overall friction coefficient, but in this case found only reasonable agreement. Ikuta et al. [16] compared computed and measured values of overall heat transfer and pressure loss for different inlet louvre designs and found good agreement. Achaichia et al. [17] investigated the variation in flow alignment with Reynolds number using the 'mean flow angle' α defined by Achaichia and Cowell [5] as a measure of the local degree of alignment. They found that the maximum value reached by α was always less than the louvre angle, but approached it at high Reynolds number. Finally, Ha et al. [18] computed the overall Nusselt number and friction factor for a limited number of louvre angle, fin pitch and Reynolds number values. They found that the Nusselt number and friction factor both increased when the louvre angle was increased or the fin pitch was reduced, but they did not attempt to compare their data with any measured values.

It can be seen that the many experiments on louvred fins over the last two or three decades have yielded valuable insight into the flow and heat transfer characteristics of these surfaces. The experiments on large-scale models, in particular, have shed much light on the relationship between the flow characteristics and the values of geometrical parameters. In developing 2-D CFD models, workers have been quick to take advantage of increases in computing power and, in some cases, the availability of commercial CFD software. With improvements in computer hardware, in particular, it has been possible to overcome restrictions on solution domain size and to develop advanced meshing arrangements giving

increased numerical accuracy. Most workers have carried out some testing of their models based on measured flow and heat transfer data. However, there appears to have been a tendency to employ data collected on large-scale models having essentially 2-D flow characteristics. In fact, there appears to have been very little testing based on overall performance data collected on practical heat exchangers. Consequently, most models have been tested in the absence of effects due to tube surface area and fin resistance. As the present paper indicates, these additional features can have a major effect on overall heat transfer parameters, with the implication that 2-D models may be inadequate for computing the heat transfer performance of practical louvred-fin heat exchangers. On the other hand, it should be said that it has only recently become possible to create 3-D models, including the effects of fin resistance, because of recent increases in computing power and the availability of commercial CFD codes capable of computing heat transfer in solid as well as fluid regions.

3. Computational models

3.1. *Conservation equations*

The flow over the louvres is assumed to be laminar and steady. In the 3-D models, variations in flow properties along all three coordinate directions are assumed to be significant. The equations representing the conservation of mass, momentum and energy (enthalpy) for the three-dimensional models are therefore as follows:

Mass

$$\frac{\partial \rho u}{\partial x}+\frac{\partial \rho v}{\partial y}+\frac{\partial \rho w}{\partial z}=0,$$

u-momentum

$$\frac{\partial \rho u^2}{\partial x}+\frac{\partial \rho uv}{\partial y}+\frac{\partial \rho uw}{\partial z}=-\frac{\partial p}{\partial x}+\frac{\partial \sigma_{xx}}{\partial x}+\frac{\partial \sigma_{xy}}{\partial y}+\frac{\partial \sigma_{xz}}{\partial z},$$

v-momentum

$$\frac{\partial \rho vu}{\partial x}+\frac{\partial \rho v^2}{\partial y}+\frac{\partial \rho vw}{\partial z}=-\frac{\partial p}{\partial y}+\frac{\partial \sigma_{yx}}{\partial x}+\frac{\partial \sigma_{yy}}{\partial y}+\frac{\partial \sigma_{yz}}{\partial z},$$

w-momentum

$$\frac{\partial \rho wu}{\partial x}+\frac{\partial \rho wv}{\partial y}+\frac{\partial \rho w^2}{\partial z}=-\frac{\partial p}{\partial z}+\frac{\partial \sigma_{zx}}{\partial x}+\frac{\partial \sigma_{zy}}{\partial y}+\frac{\partial \sigma_{zz}}{\partial z},$$

where the viscous stress terms σ_{ij} are given by

$$\sigma_{xx}=2\mu\frac{\partial u}{\partial x}+\lambda\left(\frac{\partial u}{\partial x}+\frac{\partial v}{\partial y}+\frac{\partial w}{\partial z}\right),$$

$$\sigma_{yy}=2\mu\frac{\partial v}{\partial y}+\lambda\left(\frac{\partial u}{\partial x}+\frac{\partial v}{\partial y}+\frac{\partial w}{\partial z}\right),$$

$$\sigma_{zz}=2\mu\frac{\partial w}{\partial z}+\lambda\left(\frac{\partial u}{\partial x}+\frac{\partial v}{\partial y}+\frac{\partial w}{\partial z}\right),$$

$$\sigma_{xy}=\sigma_{yx}=\mu\left(\frac{\partial u}{\partial y}+\frac{\partial v}{\partial x}\right),$$

$$\sigma_{xz}=\sigma_{zx}=\mu\left(\frac{\partial u}{\partial z}+\frac{\partial w}{\partial x}\right),$$

$$\sigma_{yz}=\sigma_{zy}=\mu\left(\frac{\partial v}{\partial z}+\frac{\partial w}{\partial y}\right),$$

Enthalpy

$$\frac{\partial \rho uh}{\partial x}+\frac{\partial \rho vh}{\partial y}+\frac{\partial \rho wh}{\partial z}=\frac{\partial}{\partial x}\left(k\frac{\partial T}{\partial x}\right)+\frac{\partial}{\partial y}\left(k\frac{\partial T}{\partial y}\right)+\frac{\partial}{\partial z}\left(k\frac{\partial T}{\partial z}\right)+u\frac{\partial p}{\partial x}+v\frac{\partial p}{\partial y}+w\frac{\partial p}{\partial z}+\Phi,$$

where the dissipation term Φ is given by

$$\Phi=\sigma_{xx}\frac{\partial u}{\partial x}+\sigma_{xy}\frac{\partial u}{\partial y}+\sigma_{xz}\frac{\partial u}{\partial z}+\sigma_{yx}\frac{\partial v}{\partial x}+\sigma_{yy}\frac{\partial v}{\partial y}+\sigma_{yz}\frac{\partial v}{\partial z}+\sigma_{zx}\frac{\partial w}{\partial x}+\sigma_{zy}\frac{\partial w}{\partial y}+\sigma_{zz}\frac{\partial w}{\partial z}.$$

In the 2-D model, the *w* component of momentum and variations in flow properties along the spanwise (*z*) coordinate direction are assumed to be zero. The conservation equations for the 2-D model are not presented here, but are obtained simply by omitting the *w* momentum equation from the preceding set of equations and deleting all terms involving *w* or derivatives with respect to *z* from the other equations in the set.

To form a closed set of equations, additional relations are required linking the thermodynamic and transport properties of the air (pressure, density, temperature, enthalpy and viscosity). Since the air can be assumed to be an ideal gas, we can make use of the ideal gas law:

$$\frac{p}{\rho}=RT.$$

In addition, for an ideal gas, the enthalpy is a function only of the temperature, and the two properties are related by

$$\mathrm{d}h=c_{\mathrm{p}}(T)\,\mathrm{d}T.$$

The change in air temperature over the fin is small, so c_{p} can be assumed constant and evaluated at the mean air temperature $(T_{\mathrm{a,i}}+T_{\mathrm{a,o}})/2$.

The viscosity of the air is also a function only of the temperature, and is obtained from Sutherland's law:

$$\mu=1.45\times10^{-6}\frac{T^{3/2}}{T+110}\ \mathrm{kg\,m^{-1}\,s^{-1}}$$

3.2. *Solution algorithm*

The preceding set of equations was solved using the commercial finite-volume computer program Star-CD.

The program solves the equations for mass, momentum and energy conservation using standard finite-volume techniques [20]. This involves subdividing the region in which the flow is to be solved into individual cells or control volumes so that the equations can be integrated numerically on a cell-by-cell basis to produce discrete algebraic (finite-volume) equations. The program offers a range of numerical schemes with which to approximate the convection terms in the equations, e.g. central differencing, linear upwind differencing, self-filtered central differencing (SFCD) [21, 22]. The SFCD scheme was used for all of the equations as this appeared to give the best compromise between numerical accuracy and stability of the solution algorithm. Several algorithms for calculating the pressure field are available in the program (SIMPLE, PISO, SIMPISO, see e.g. [23]). For these steady-state computations, the SIMPLE algorithm was found to give the shortest computer running times and was used in all of the calculations.

3.3. Numerical meshes

To create the numerical meshes, two Fortran computer programs were written, one for the 2-D model and the other for the 3-D models. The programs read in the geometric parameters of the fin and created a file containing the coordinates of the corners of all of the cells which made up the mesh. This file could be read by the Star-CD pre-processor, prostar, which assembled and displayed the mesh.

In all of the models the mesh was constructed around only one fin, since the fin was assumed to be an element of an array. The flow along the top and bottom surfaces of the mesh was assumed to be cyclic. In the version of Star-CD used, cyclic conditions could only be applied to pairs of boundaries having identical mesh structures. The Fortran programs were therefore written to meet this requirement.

All of the models had the same mesh structure in the x–y plane (perpendicular to the fin surface). In fact, a large part of the creation of the mesh for the 3-D models consisted of simply duplicating the basic 2-D mesh and stacking the individual meshes to form a 3-D structure. The creation of the mesh for the 2-D model will therefore be considered first.

3.3.1. Two-dimensional model

The basic 2-D mesh had a block structure, with three different types of block corresponding to the inlet section of the fin, the individual louvres, and the turn-around section (see Fig. 2). To create the mesh, each block was first subdivided into smaller blocks which were then subdivided into individual quadrilateral cells. Once the mesh for the first half of the fin had been constructed, the second half, which was just a mirror image of the first, was constructed by simply duplicating the first half and rotating the duplicate mesh through 180°.

This type of mesh structure, consisting of a set of blocks divided into quadrilateral cells, has several important advantages:

- the block structure means that it is quick and easy to create meshes for fins containing many louvres;
- the mesh around each louvre is the same (apart from the louvres contained in the inlet/outlet and turn-around blocks), making it easy to compare the flow and heat transfer over one louvre with that of another;
- mesh lines are normal to the louvres, making it easy to extract boundary layer profiles and calculate integral parameters;
- nearly all of the mesh cells are square, giving maximum numerical accuracy.

With the Fortran computer program it was possible to create meshes for most fin geometries of practical interest. Figure 3 shows the mesh structure around the inlet/outlet section, the individual louvres, and the turn-around section of a practical fin geometry.

The cells in the 2-D mesh were approximately uniform in size. In the computations, two cell sizes were used, one roughly equal to the fin thickness ($t = 0.05$ mm), and the other roughly equal to half the fin thickness. The effect on the flow solutions of refining the mesh will be discussed in Section 5. The total number of mesh cells used depended on the values of the geometric parameters, but was typically 35 000 for coarse-mesh computations and 135 000 for fine-mesh computations.

3.3.2. Three-dimensional models

Most of the 3-D computations were carried out using a basic 3-D model which incorporated the effects of heat transfer from the tube surfaces, but neglected the tube width and therefore flow accelerations and decelerations around the tubes. A limited number of computations were carried out using a slightly more realistic model in which the tube width was represented. However, to simplify the meshing process, the rounded corners of the tubes were modelled (somewhat crudely) by 90° corners (Fig. 4). In both models the louvres were assumed to extend the whole width of the flow passage between the tubes, thus ignoring the thin strip of unlouvred material which in practice exists between the tubes and the ends of the louvres. Manufacturers generally aim to make this unlouvred area as small as possible, and, as discussed in Section 5, the effect on the computations of ignoring it is not likely to be significant, except possibly for geometries with small tube pitch where the unlouvred area is proportionally greater.

To create the mesh for the simpler 3-D model (model A), it was necessary only to duplicate the 2-D mesh several times and to stack the duplicate meshes. The width of the mesh was arranged to be equal to half of the width

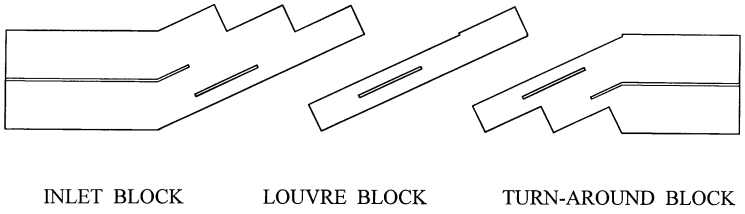

Fig. 2. Block structure of the 2-D mesh.

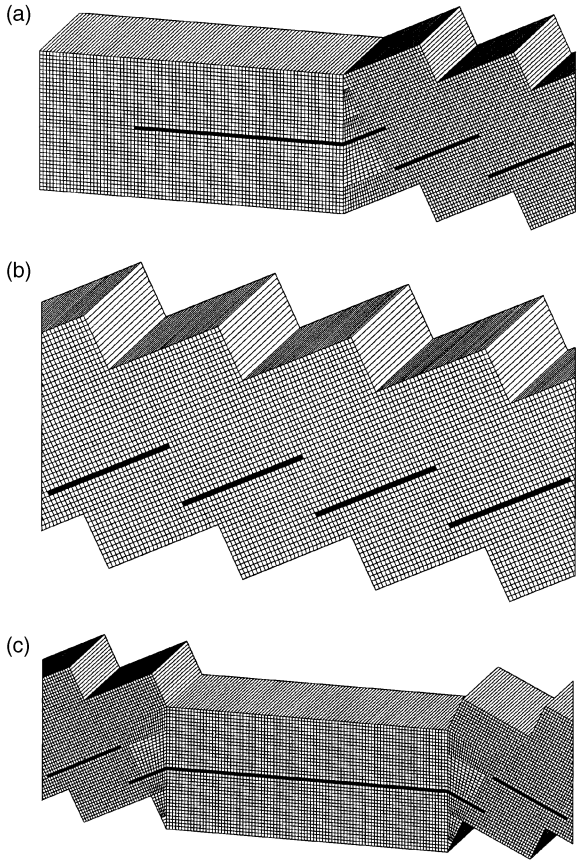

Fig. 3. Typical mesh for the 2-D model; $F_p = 2.054$ mm, $L_p = 1.4$ mm, $\theta = 25.5^\circ$, $t = 0.05$ mm. (a) Inlet section. (b) Individual louvres. (c) Turn-around section.

of the passage between the tubes, i.e. $(T_p - T_w)/2$, where T_p is the tube pitch and T_w is the tube width. One side of the mesh was defined to be a symmetry plane and the side opposite was divided into symmetry planes and solid regions, as shown in Fig. 4. The width of the solid regions was equal to the distance between the farthest upstream and downstream points on the outer surfaces of the tubes.

In the computations, one value of tube width, equal to 2 mm, and two values of tube pitch, equal to 8 and 14 mm, were considered. In each case, the width of the cell layer adjacent to the tube wall was set equal to the fin thickness (0.05 mm), and the remaining cell layers expanded in width towards the symmetry plane. The expansion factor was arranged to be no greater than 1.2, giving a total of 15 cell layers for the tube pitch 8 mm and 19 cell layers for the tube pitch 14 mm.

The mesh for the more realistic model (model B) was developed from the mesh for model A. The three surfaces defined as symmetry planes on one side of model A were displaced sideways into the centreplane of the tubes, and the spaces in between were filled by duplicating and stacking the adjacent mesh structure. The spacing between the cell layers was arranged to expand uniformly to the centreplane. With the number of cell layers set to 9, the expansion factor was almost exactly 1.2. As in the 2-D model, the total number of mesh cells depended on the values of the geometric parameters. For the computations with tube pitch 8 mm the total number of cells was around 500 000 for model A and 560 000 for model B.

3.4. Boundary conditions

Boundary conditions were required for u, v and T in the 2- and 3-D models, and also for w in the 3-D models. At the inlet plane all of the properties were assumed to be constant, with v (and w in the 3-D models) being set to zero and T being set to the ambient atmospheric temperature.

On the fin and tube surfaces, no-slip (i.e. zero velocity) conditions were assumed to exist. In the 2-D model the temperature of the fin was assumed to be constant and to be about 70°C above the atmospheric temperature. This corresponded to the difference in air and water-side temperatures in the experiments by Achaichia and Cowell [3].

In the 3-D models the temperature of the tube surface was assumed to be 70°C above the atmospheric temperature. The Star-CD program has the facility to compute the temperature distribution within both solid and fluid regions, and in the 3-D models this facility was used to compute the variation in temperature in the fin with distance from the tube surface. The fall in temperature across the fin was found to be significant under certain flow conditions, and to lead to significantly better agreement between the predicted and experimentally deter-

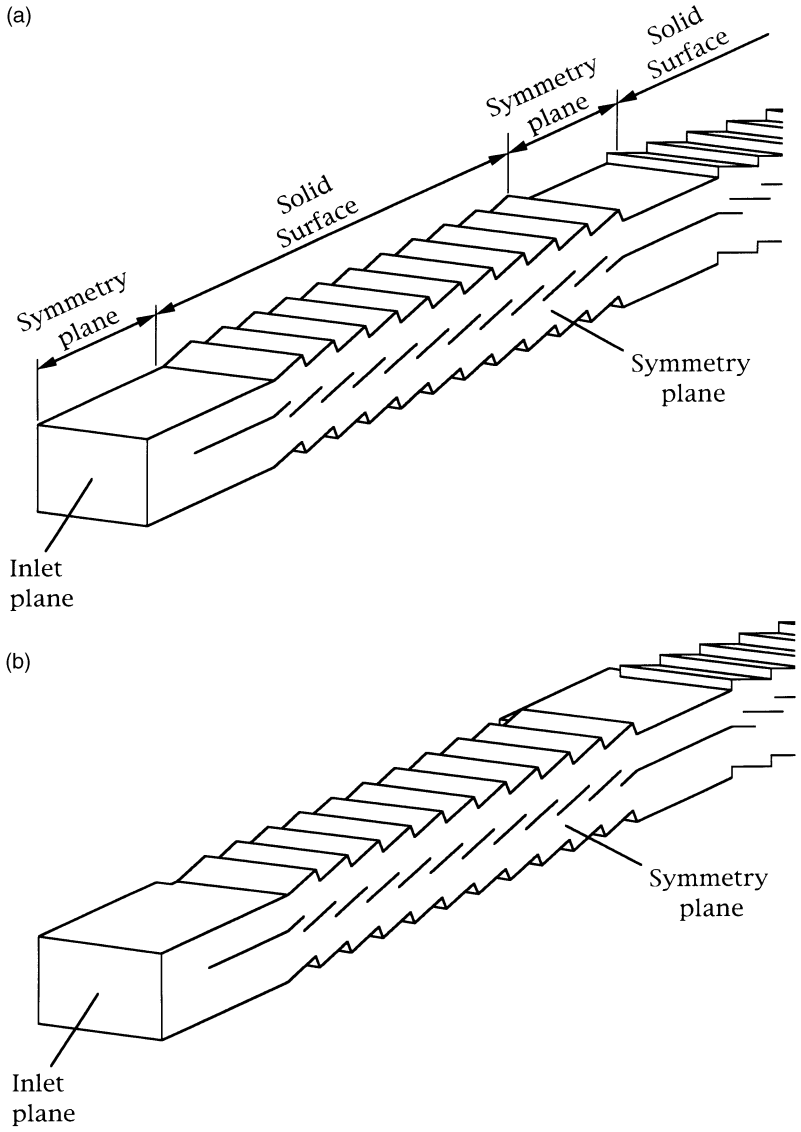

Fig. 4. Solution domains for the 3-D models. (a) Model A. (b) Model B.

mined heat transfer performance. The effect of the fin temperature calculation on the flow solutions is discussed in more detail in Section 5, but it may be stated here that this facility appears to be an essential component in the correct modelling of louvred-fin flows.

4. Determination of performance parameters

The pressure drop and heat transfer performance of the louvred fin for a given set of geometric and flow conditions can be characterised by a friction factor and a Stanton number, respectively. The flow conditions themselves can be characterised by a Reynolds number, while the geometric conditions can be characterised in terms of dimensionless parameters such as fin-to-louvre pitch ratio and louvre angle.

Following the conventions laid down by Kays and London [24], the friction factor and Stanton number are defined in terms of the heat transfer area A_a, the minimum flow area A_c, and the mean velocity through the minimum flow area U, as follows:

$$f = \frac{\Delta p}{\frac{\rho U^2}{2}\frac{A_a}{A_c}}, \quad St = \frac{h_c}{\rho U c_p}.$$

The heat transfer coefficient h_c appearing in the Stanton

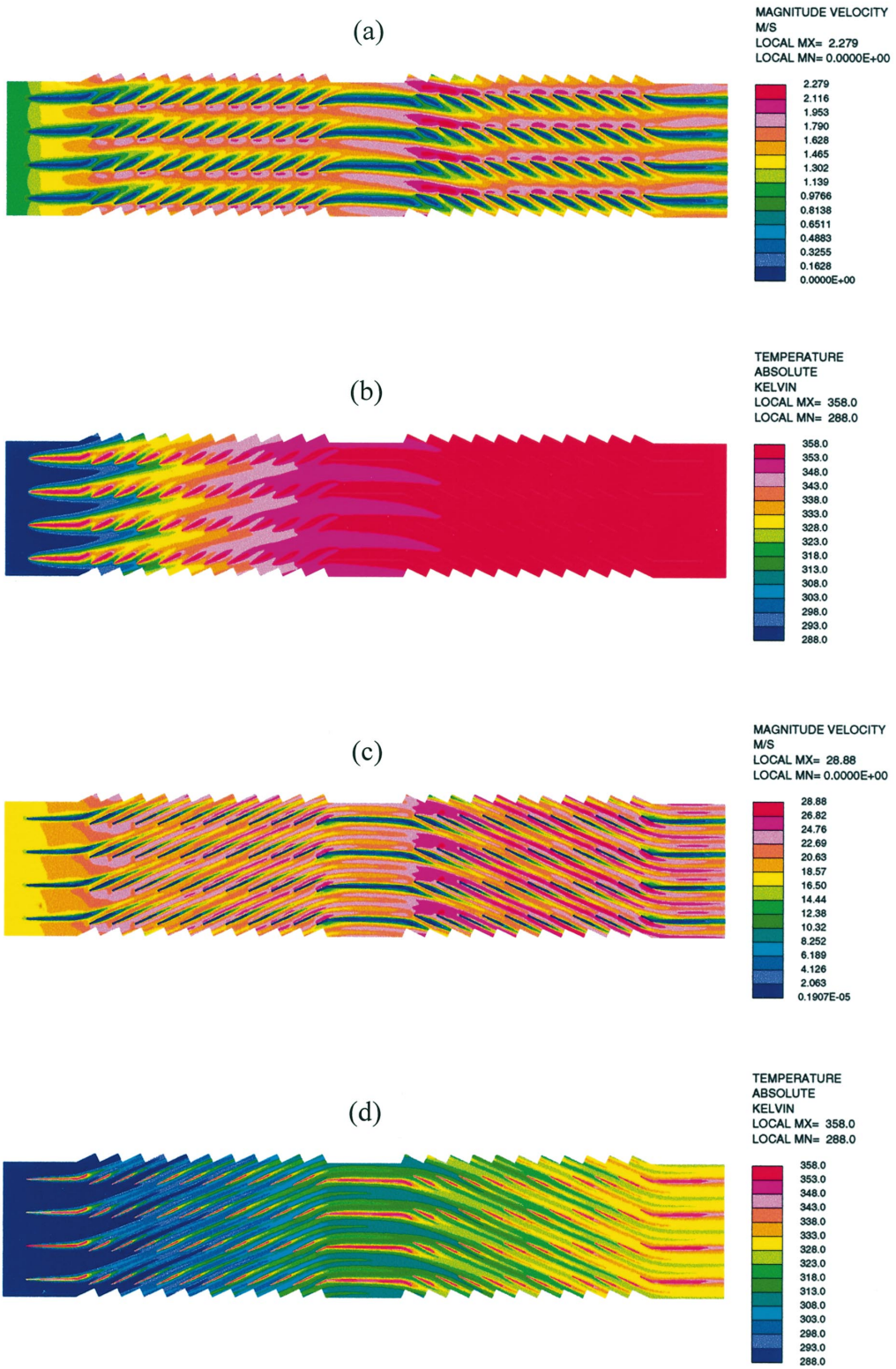

Fig. 5. Computed velocity and temperature fields for the 2-D model; $F_p = 2.054$ mm, $L_p = 1.4$ mm, $\theta = 25.5^\circ$, $t = 0.05$ mm. (a) Velocity, $Re_{Lp} = 100$. (b) Temperature, $Re_{Lp} = 100$. (c) Velocity, $Re_{Lp} = 1600$. (d) Temperature, $Re_{Lp} = 1600$.

number is defined in terms of the heat flux Q and the logarithmic mean temperature difference $LMTD$:

$$h_c = \frac{Q}{A_a LMTD}, \quad LMTD = \frac{\Delta T_o - \Delta T_i}{\ln(\Delta T_o/\Delta T_i)}.$$

The heat flux Q is given by

$$Q = mc_p(T_{a,o} - T_{a,i}) = \rho U A_c c_p (T_{a,o} - T_{a,i}).$$

Hence

$$h_c = \rho U c_p \frac{A_c}{A_a} \frac{(T_{a,o} - T_{a,i})}{LMTD}$$

and

$$St = \frac{h_c}{\rho U c_p} = \frac{A_c}{A_a} \frac{(T_{a,o} - T_{a,i})}{LMTD}.$$

By convention the Reynolds number is defined in terms of the hydraulic diameter D_h:

$$Re_{Dh} = \frac{\rho U D_h}{\mu}.$$

However, Achaichia and Cowell [3] found that correlating their friction factor and Stanton number data with Reynolds number was made easier if the Reynolds number was defined in terms of the louvre pitch L_p, i.e.

$$Re_{Lp} = \frac{\rho U L_p}{\mu}.$$

In the 2-D model the area ratio A_c/A_a becomes $(F_p - t)/2L$, where L is the fin length, F_p is the fin pitch, and t is the fin thickness. The friction factor and Stanton number are then defined by

$$f = \frac{\Delta p(F_p - t)}{\rho U^2 L}, \quad St = \frac{(F_p - t)}{2L} \quad \frac{(T_{a,o} - T_{a,i})}{LMTD}.$$

The flow field around the louvred fins is only affected by the heat transfer via the latter's effect on fluid properties. For the temperature range in automotive heat exchangers this effect is small and the flow field is almost independent of the heat transfer. In fact, in their experiments, Achaichia and Cowell [3] followed conventional practice and obtained their friction factor results from separate experiments on isothermal air flows. Thus to evaluate the numerical models it was necessary to carry out two sets of computations, one for isothermal flow, and the other for variable temperature flow. As a consequence, the pressure drop predictions (and the degree to which they agree with experiments) are entirely independent of the heat transfer predictions.

5. Results of computations

5.1. *Two-dimensional model*

5.1.1. *Flow and heat transfer characteristics*

Before an evaluation of the 2-D model is carried out, an examination of computed results for a typical fin geometry will be made in order to gain insight into the flow and heat transfer characteristics of the fin and the influence of the Reynolds number. The geometry chosen for this study was the first to be tested by Achaichia and Cowell [3] and had a fin pitch of 2.054 mm, louvre pitch of 1.4 mm, louvre angle of 25.5°, fin thickness of 0.05 mm and tube pitch of 11 mm. As mentioned in Section 3, computations with the 2-D model were carried out for two different meshes, one a 'coarse' mesh with cell sizes roughly equal to the fin thickness, and the other a 'fine' mesh with cell sizes roughly equal to half the fin thickness. The following illustrative results are for the coarse mesh, but are almost identical to those for the fine mesh.

Figure 5 shows the computed velocity and temperature fields around the fin for two different Reynolds numbers, 100 and 1600. At a Reynolds number of 100 (Figs. 5a and 5b), much of the air flows through the channels between the fins rather than through the louvres, as indicated by the presence of high-velocity streaks in the channels. The thick boundary layers on the louvres serve to block the louvre passages and prevent the flow of air. The temperature of the air can be seen to reach the fin temperature before the air leaves the fin, so the heat transfer performance of the fin is poor. In fact, the second half of the fin simply causes a pressure loss without producing any heat transfer. At a Reynolds number of 1600 (Figs. 5c and 5d) the louvre boundary layers are much thinner, and so the air is diverted through the louvre passages. A temperature difference is maintained between the air and the fin, and so every part of the fin contributes to the heat transfer.

A very effective way to illustrate the change in flow characteristics with Reynolds number is to plot the paths of individual fluid particles. Figure 6 presents these particle paths for three different Reynolds numbers, 10, 100 and 1600. In each case, ten particles are considered originating from uniformly spaced locations across the inlet plane. At a Reynolds number of 10, each louvre deflects only one particle, and so all ten particles are deflected only after the tenth louvre. It is also interesting to note how each particle is forced into the centre of the louvre passage by the boundary layer growth. At a Reynolds number of 100, two or three particles are deflected by each louvre, and finally, at a Reynolds number of 1600, all of the particles are deflected by the first two or three louvres. If the flow is parallel to the louvres then it is possible to predict the maximum vertical distance each particle will travel, given the louvre angle and the length of each louvre bank. For the fin chosen, these parameters are 25.5° and 15.4 mm, respectively. The maximum vertical distance will therefore be about 7.3 mm (or approximately $3\frac{1}{2}$ fin pitches for the fin chosen), and this is roughly the case in Fig. 6c.

5.1.2. *Overall friction factor and Stanton number*

The overall friction factor and Stanton number were determined for the fin geometry used in the preceding

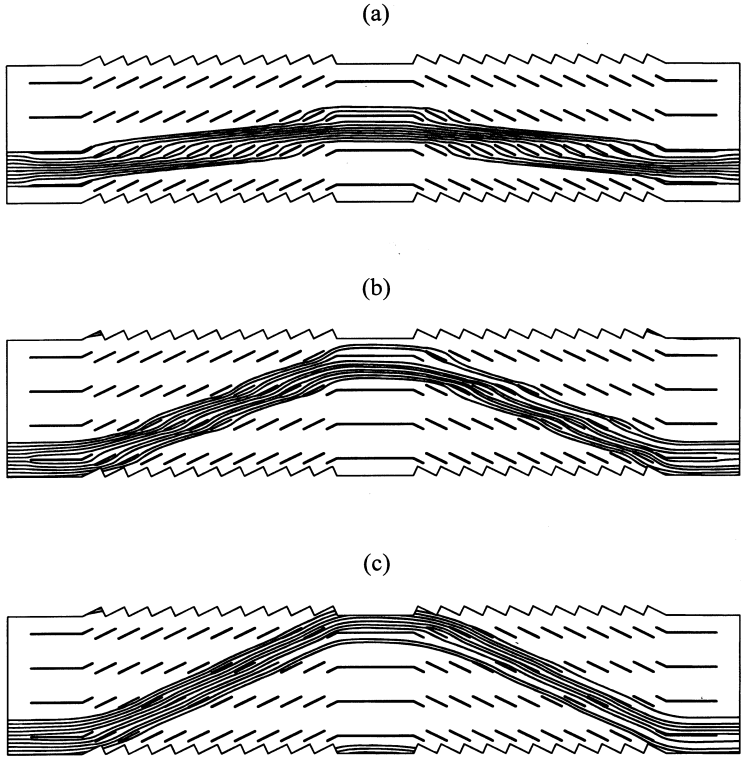

Fig. 6. Particle paths for a louvred fin. (a) $Re_{Lp} = 10$. (b) $Re_{Lp} = 100$. (c) $Re_{Lp} = 1600$.

computations, using the equations given in Section 4 for the limiting case of two-dimensional flow. Numerical computations were made for Reynolds numbers from 100 to 3200, and therefore over a somewhat greater range than is typical of automotive heat exchangers ($Re_{Lp} = 200$ to 1200). In Fig. 7a, the friction factor and Stanton number for both the coarse and fine mesh solutions are plotted against Reynolds number, along with the experimentally determined values of Achaichia and Cowell [3]. The coarse and fine mesh results can be seen to be very similar, except for a slight lowering of the Stanton number with mesh refinement at high Reynolds number. The computed results appear to be relatively insensitive to mesh refinement, given that a two-fold reduction in the cell size was carried out. Since the SFCD scheme used in the computations is approximately second-order accurate, any further changes with mesh refinement can be expected to be small. It therefore seems reasonable to suppose that the computed results (at least for the fine mesh) are close to being mesh independent.

From Fig. 7a it can be seen that the computed friction factor and Stanton number follow very similar trends to the measurements. The measured friction factor and Stanton number have roughly constant slope for Reynolds numbers greater than 200, when plotted on log–log axes, and this trend is also reflected in the calculations, with the computed slope being almost exactly the same as in the measurements. However, it is clear from Fig. 7a that there is a significant offset between the computed and measured Stanton number. This offset is uniform and represents a 70% overprediction of the Stanton number, and hence the heat transfer rate. Also evident is the fact that no computed Stanton number data are plotted for a Reynolds number of less than 200, even though the measured data (and the computed friction factor data) continue down to a Reynolds number of 100. Both the offset in the Stanton number and the absence of computed Stanton number data at low Reynolds numbers are essentially due to the fact that the heat transfer rate is overpredicted. This overprediction causes the air temperature to reach the fin temperature at low Reynolds number, as seen in Fig. 5b, which in turn causes ΔT_o to become zero and the $LMTD$ to become indeterminate.

Computations were not made for Reynolds numbers below 100, but it can be seen from Fig. 7a that the slope of the measured friction factor data increases significantly for lower Reynolds numbers. Achaichia and Cowell [3] attribute this increase in slope to the change in flow alignment at low Reynolds number. Consequently, the slope of the friction factor data ceases to be consistent

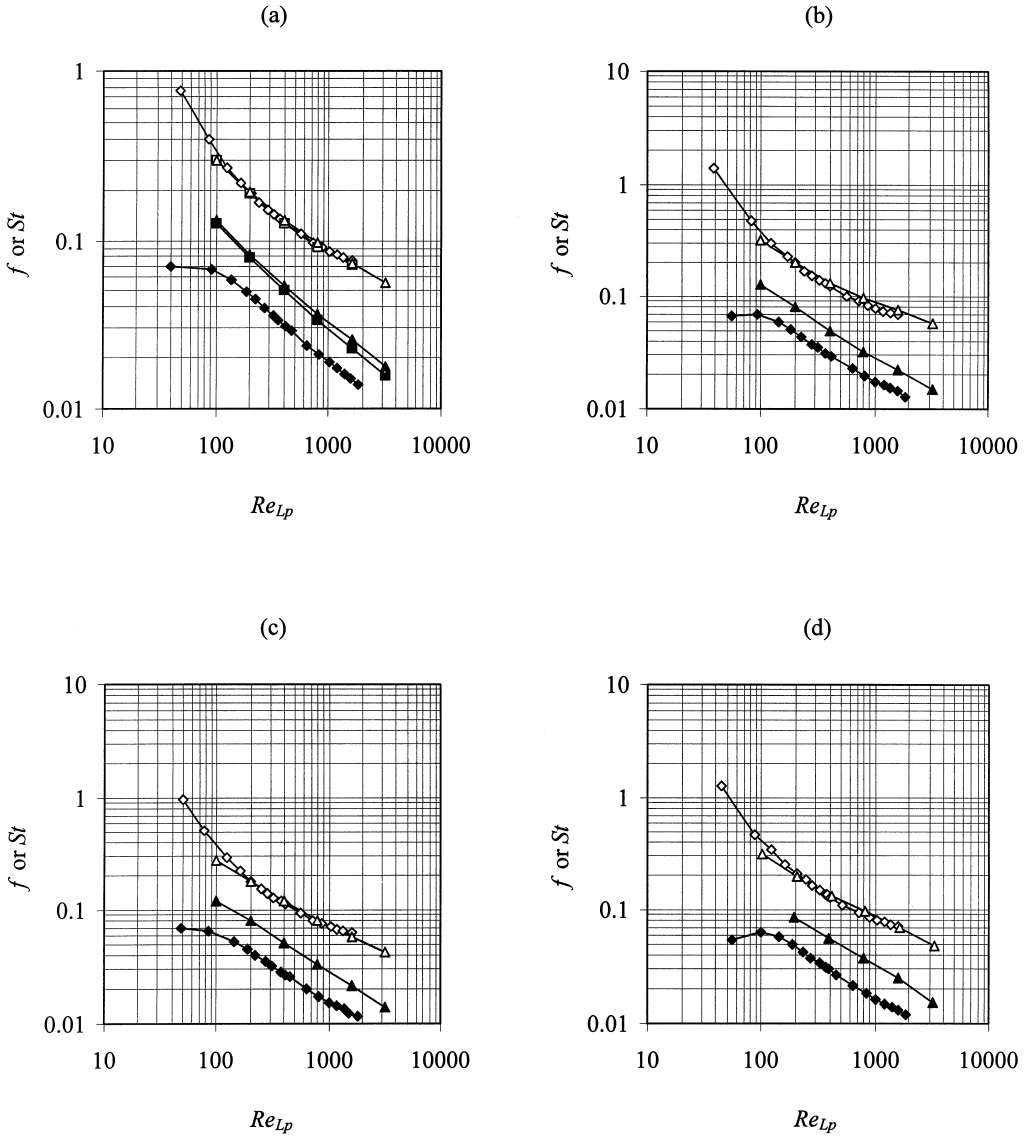

Fig. 7. Computed and measured friction factor and Stanton number. Computations are for the 2-D model. Friction factor: △, computed, coarse mesh; □, computed, fine mesh; ◇, measured. Stanton number: ▲, computed, coarse mesh; ■, computed, fine mesh; ◆, measured. Data are shown for $L_p = 1.4$ mm, $T_p = 11$ mm, $t = 0.05$ mm and (a) $F_p = 2.05$ mm, $\theta = 25.5°$; (b) 2.04 mm, 28.5°; (c) 2.09 mm, 21.5°; (d) 1.64 mm, 25.5°.

with a series of laminar boundary layers and approaches a value more consistent with laminar flow in a rectangular channel.

Further computations were made for some of the other fin geometries investigated by Achaichia and Cowell [3]. The geometries chosen for these computations encompassed a wide variety of individual geometric parameter values, and comparisons of computed and measured friction factor and Stanton number for some for the geometries are shown in Figs. 7b–d. In all cases the model's performance in terms of friction factor and Stanton number does not appear to be very different from its performance for the first geometry (Fig. 7a). The friction factor is computed reasonably well for all of the geometries, but the Stanton number is always significantly overpredicted, although, as with the first geometry, the slope of the computed Stanton number data agrees well with the measured slope. The size of the offset was found to vary from one geometry to another, and to reach as high as 100% for some geometries.

5.1.3. Local Nusselt number

Experimental values of local Nusselt number for a louvred fin geometry were obtained by Antoniou [25]. The experiments were carried out on a scale model roughly four times the size of a practical louvred fin, and the Nusselt number values were deduced from mass transfer measurements involving the sublimation of naphthalene. Realistic Reynolds number values of 550, 1000 and 2000 were achieved by reducing the air velocity to a quarter of practical values. Computations were made for all three Reynolds numbers, and comparisons of computed and measured local Nusselt number values for a Reynolds number of 550 are shown in Fig. 8. The trends in the computations and measurements can be seen to be very similar, with the Nusselt number falling rapidly over each louvre before rising slightly at the end of each louvre. The rise in Nusselt number is due to flow impingement and local flow acceleration as the air enters the gap between louvres. The computed and measured values can be seen to differ on the downstream part of each louvre, but quantitative agreement is not expected given the considerable difficulties involved in determining the local heat transfer from mass transfer measurements [25].

Overall, it can be seen that the 2-D model yields reasonably accurate predictions of friction factor, but poor predictions of Stanton number, with the latter parameter being significantly overpredicted. The computed Stanton number values clearly depend on the predicted heat transfer rate, and the errors in these quantities can be attributed to the overprediction of the heat transfer rate, or more precisely, the heat transfer rate per unit area, Q/A_a. An obvious way to identify the sources of error in the heat transfer is to consider the practical features which are missing from the 2-D model. Two important features which are missing are the tube surfaces and the fin resistance. The tube surfaces would add to the heat transfer area A_a, but would not add significantly to the overall heat transfer rate Q because of the thick boundary layer growth on the tubes. The fin resistance would lower the temperature across the fin, and thus the heat transfer from the fin. It is these factors which led to the development of the 3-D models.

5.2. *Three-dimensional models—model A*

5.2.1. Flow and heat transfer characteristics

To evaluate model A, further use was made of the experimental data of Achaichia and Cowell [3]. Two fin geometries were selected which were identical apart from the tube spacing, which was 8 mm for one geometry and

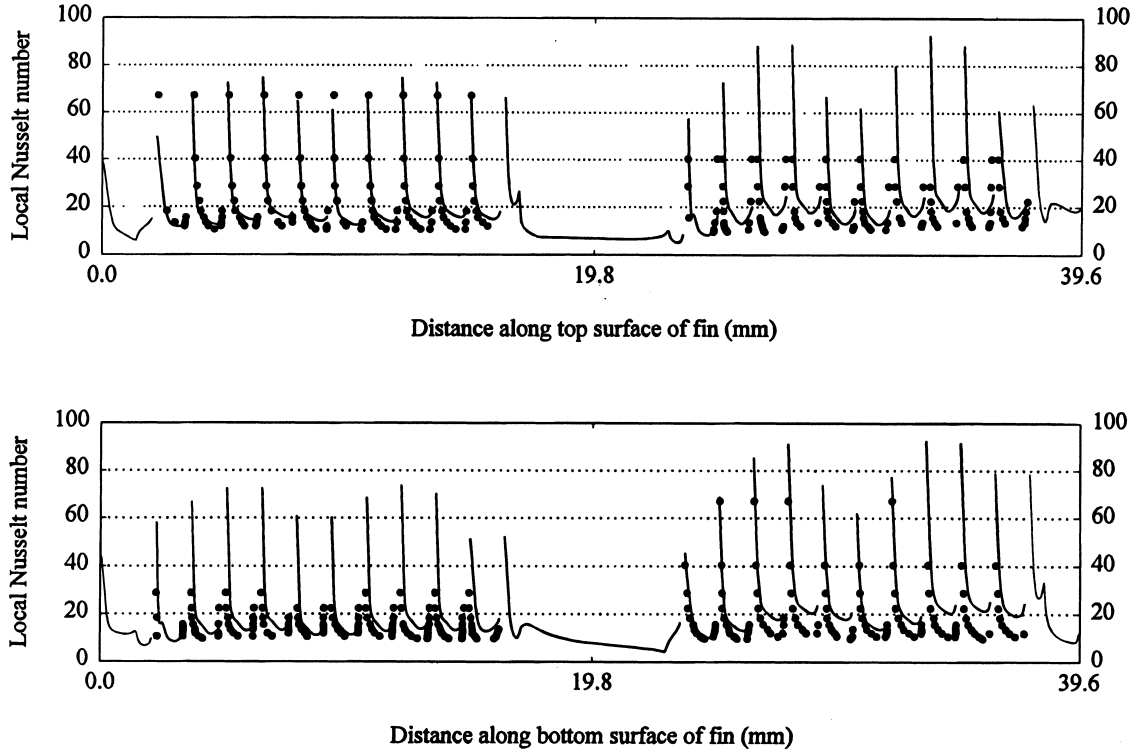

Fig. 8. Computed and measured local Nusselt number ($Nu = h_c L_p/k$); $Re_{Lp} = 550$, $\Delta T = 70$ K, $F_p = 2.375$ mm, $L_p = 1.4$ mm, $t = 0.125$ mm; —, computed; ●, measured.

14 mm for the other. The other dimensions were: fin pitch 2.17 mm, louvre pitch 1.1 mm, louvre angle 22°, and fin thickness 0.05 mm. Computations were made for Reynolds numbers between 100 and 1600.

The velocity and temperature distributions away from the tube walls were found to be very similar to those in the 2-D computations and to vary in the same way with Reynolds number. The velocity field was essentially two-dimensional, except in the boundary layers growing on the tube walls. The thickness of these boundary layers was found to be uneven because of the presence of the louvres, but to be essentially independent of the tube spacing, and to decrease with Reynolds number, as expected. From the computed velocity field, the thickness of the velocity boundary layer was determined at the downstream edge of the solid surface representing the second (downstream) tube. The thickness was found to decrease from about 0.9 mm at a Reynolds number of 100 to about 0.5 mm at a Reynolds number of 1600. The contributions to the total heat transfer from the tubes and the fin were determined for each Reynolds number, and these values were used to determine the reduction in Q/A_a due to the presence of the tube surfaces. These reductions varied from 14 to 13% with increasing Reynolds number for the geometry with tube pitch 8 mm, and from 8 to 6% for the geometry with tube pitch 14 mm.

5.2.2. Fin temperature variation

The temperature of the fin was found to decrease with distance from the tubes because of the fin resistance, and by an amount which increased significantly with Reynolds number. In Fig. 9 the variation in fin temperature is plotted for two locations along the fin corresponding to the middle of the two tubes. The temperature falls more at the upstream location because the air temperature is lower, and as would be expected, the temperature in the middle of the fin falls further as the tube spacing is increased. The rapid fall in temperature at high Reynolds number can be attributed to the higher heat transfer coefficient on the fin surface.

5.2.3. Overall friction factor and Stanton number

In Fig. 10 computed and measured values of friction factor and Stanton number for the two fins are presented. Computed values for both the 2-D model and the 3-D model are included to indicate the improvement made by the 3-D model. Also shown, for a Reynolds number of 400, is the computed Stanton number when the fin temperature is assumed to be uniform (i.e. the fin resistance is assumed to be zero). This latter value serves to indicate the improvement in Stanton number due to the inclusion of the fin resistance.

It can be seen that the 3-D model produces even closer agreement between computed and measured friction factor, particularly for the tube pitch of 8 mm. The results

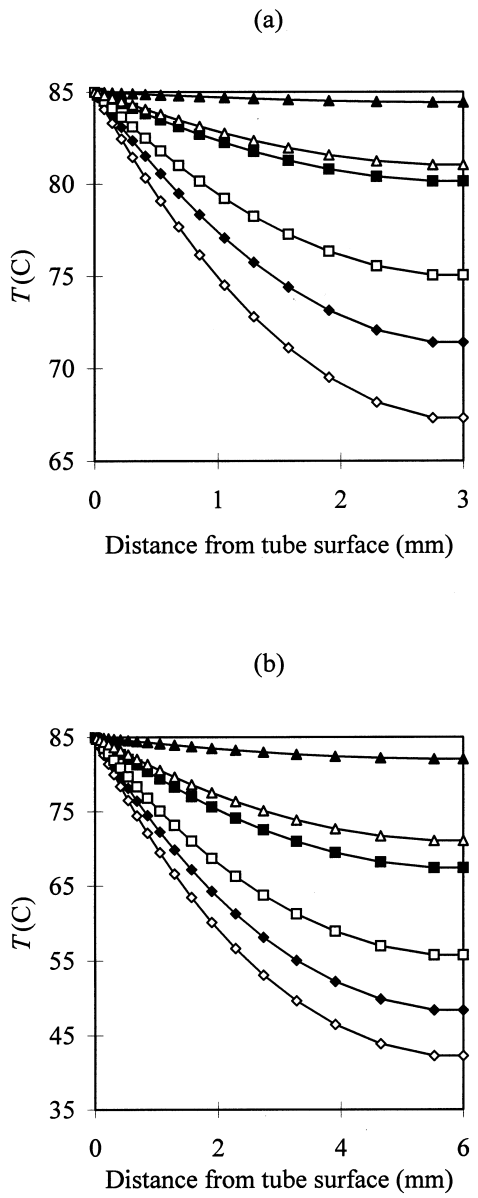

Fig. 9. Computed temperature variation across the fin; $F_p = 2.17$ mm, $L_p = 1.1$ mm, $\theta = 22°$, $t = 0.05$ mm. Middle of upstream tube: Δ, $Re_{Lp} = 100$; □, 400; ◇, 1600; middle of downstream tube; ▲, $Re_{Lp} = 100$; ■, 400; ◆, 1600. (a) $T_p = 8$ mm. (b) $T_p = 14$ mm.

for the 2-D model are independent of the tube spacing, and the differences between computation and measurement for the lower tube pitch are more pronounced because of the influence of the tube spacing. It is noteworthy that the 3-D model produces a greater change in friction factor at the lower tube pitch as required to achieve agreement.

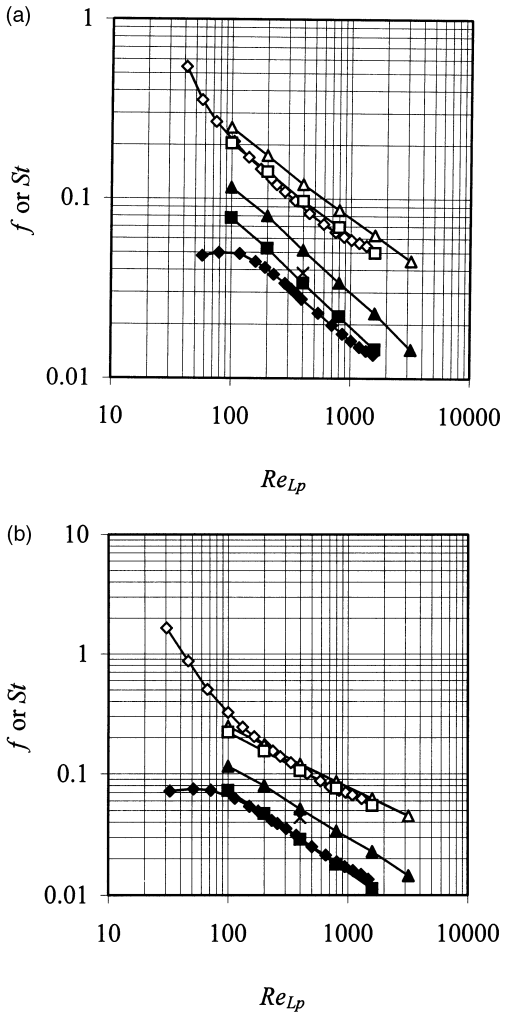

Fig. 10. Computed and measured friction factor and Stanton number. Friction factor: △, computed, 2-D model; □, computed, 3-D model A; ◇, measured. Stanton number: ▲, computed, 2-D model, ■, computed, 3-D model A; X, computed, 3-D model A with uniform fin temperature; ◆, measured. $F_p = 2.17$ mm, $L_p = 1.1$ mm, $\theta = 22°$, $t = 0.05$ mm. (a) $T_p = 8$ mm. (b) $T_p = 14$ mm.

The use of the 3-D model can be seen to bring about a considerable reduction in the offset in Stanton number. For the tube pitch of 14 mm the offset is practically reduced to zero, while for the tube pitch of 8 mm it is reduced from a value representing a 90% error to a value representing a 25% error. One possible reason for the remaining error is lack of mesh refinement. The cell sizes in the x-y plane of the 3-D mesh were the same as those in the 2-D coarse mesh, and Fig. 7a shows that refining the mesh in the x-y plane can produce a further significant reduction in the offset (around 15%). Another possible reason is that the model ignores the thin strips of unlouvred material adjacent to the tubes. It is possible that ignoring these strips might cause the heat transfer to be overpredicted in rough proportion to the width of the strips. According to Achaichia and Cowell [3] the strips were about 1/4 mm in width. For the tube pitch of 8 mm they accounted for about 8% of the width of the flow passage (leading to a possible 8% overprediction of the Stanton number), and for the tube pitch of 14 mm, about 4%. Achaichia and Cowell estimated that the uncertainties in their Stanton number and friction factor data were about 6.5 and 15%, respectively, at the lower end of the Reynolds number range in Fig. 10, and about 3.5 and 5%, respectively, at the upper end of the range.

From Fig. 10, it can be seen that the inclusion of the fin resistance makes a significant contribution to the improvement in the computed Stanton number. For the tube pitch of 8 mm the contribution is 27%, and for the tube pitch of 14 mm it is 65%. These results are consistent with the lower overall fin temperature for the wider tube pitch (Fig. 9), and serve to emphasise the importance of modelling the fin resistance, especially for heat exchangers with wide tube spacing.

5.3. Three-dimensional models—model B

Model B was applied to a single fin geometry, this being the geometry with tube pitch 8 mm used to evaluate model A. Computations were carried out for Reynolds numbers of 100, 400 and 1600, but it was found that converged solutions could only be obtained for the Reynolds numbers 100 and 400. The computed Stanton number values for the two Reynolds numbers were found to be very close to those for model A (within 4%), and this was thought to be due to the fact that the inclusion of the tube width does not affect Q/A_a significantly. The computed friction factor values were found to be somewhat higher than those for model A (by 11% at $Re_{Lp} = 400$) and therefore in poorer agreement with measurements. However, it is thought that much of the increase was due to the rather crude modelling of the tube corners, and in fact ignoring the tube width, as in model A, leads to a more accurate estimation of the pressure loss.

An examination of the velocity field around the tubes revealed regions of separated flow at the corners of the tubes. It was thought that the lack of convergence at Reynolds number 1600 was due essentially to the fact that these separation regions become unsteady at high Reynolds number. Solving steady-flow equations is therefore no longer appropriate. It is possible that convergence could have been achieved if the rounded corners of the tubes had been accurately represented, but the results for friction factor and Stanton number would appear to call into question the value of modelling these corners at all.

In summary, it can be seen that the 3-D models give significantly better predictions of performance par-

ameters than the 2-D model, and that predictions of the Stanton number in particular are substantially better with the 3-D models. For the geometry with tube pitch 8 mm, differences were still present between computed and measured Stanton number. Two possible sources of error in the computations were identified. Lack of mesh refinement was thought to be a significant source of error, and the fact that the unlouvred area of the fin was ignored may also have been significant, since this area accounts for a greater proportion of the fin area for geometries with small tube pitch.

6. Conclusions

In this paper 2- and 3-D numerical models have been described for computing the flow and heat transfer over louvred fin arrays in compact heat exchangers. Two 3-D models were presented, both of which incorporated the tube surface area and the fin resistance, and one of which incorporated the tube width. The models were evaluated using the measurements of overall Stanton number and friction factor for louvred fin heat exchangers by Achaichia and Cowell [3].

It was found that the tube surface area and fin resistance in the 3-D models led to a considerable lowering of the predicted heat transfer rate per unit area (Q/A_a), and as a result the 3-D models gave much more accurate predictions of overall Stanton number than the 2-D model. All of the models gave satisfactory predictions of overall friction factor, although it was noted that for one fin geometry with small tube pitch the 3-D models gave significantly better predictions than the 2-D model. The effect on the Stanton number of modelling the tube width was negligible, and this finding was thought to be due to the fact that the inclusion of the tube width does not affect Q/A_a significantly. It was found that the inclusion of the tube width led to slightly poorer predictions of the friction factor, contrary to expectations, but it was thought that the slightly poorer results could be attributed to the rather crude way in which the tube corners were modelled. For the fin geometry with small tube pitch it was found that significant differences were still present between computed and measured Stanton number even when the 3-D models were used. Apart from measurement uncertainties, two possible sources of error were identified. These were lack of mesh refinement and the fact that in the computations no account was taken of the unlouvred area of the fin adjacent to the tubes.

The computing resources required by the 3-D models were considerably greater than those of the 2-D model, with run times for the 3-D models being typically ten times those of the 2-D model (about 20 hours on the Silicon Graphics computer). Nevertheless, it is argued that the superior heat transfer predictions of the 3-D models makes them much more useful as design tools than the 2-D model. In any case, if the recent rapid increases in computing power continue, there is every likelihood that the run times of the 3-D models will, within the very near future, match those of 2-D models on today's computers.

References

[1] C.J. Davenport, Heat transfer and fluid flow in louvred triangular ducts: PhD thesis. CNAA, Lanchester Polytechnic, 1980.
[2] C.J. Davenport. Heat transfer and flow friction characteristics of louvred heat exchanger surfaces, in: J. Taborek, G.F. Hewitt, N. Afgan, (Eds), Heat Exchangers, Theory and Practice, Hemisphere/MacGraw-Hill, Washington, DC, 1983, pp. 397–412.
[3] A. Achaichia, T.A. Cowell. Heat transfer and pressure drop characteristics of flat tube and louvred plate fin surfaces. Experimental Thermal and Fluid Science 1 (1988) 147–157.
[4] M. Kajino, M. Hiramatsu. Research and development of automotive heat exchangers, in: W.J. Yang, Y. Mori (Eds.), Heat Transfer in High Technology and Power Engineering, Hemisphere, Washington, DC, 1987, pp. 420–432.
[5] A. Achaichia, T. A. Cowell. A finite difference analysis of fully developed periodic laminar flow in inclined louvre arrays. Proceedings of the Second U.K. National Heat Transfer Conference, 1988, pp. 883–898.
[6] F.N. Beauvais. An aerodynamic look at automotive radiators. SAE Paper No. 650470, 1965.
[7] L.T. Wong, M.C. Smith. Airflow phenomena in the louvered-fin heat exchanger. SAE Paper No. 730237, 1973.
[8] R.L. Webb, P. Trauger. Flow structure in the louvered fin heat exchanger geometry. Experimental Thermal and Fluid Science 4 (1991) 205–217.
[9] A.A. Antoniou, M.R. Heikal, T.A. Cowell. Measurements of local velocity and turbulence levels in arrays of louvred plate fins. Proceedings of the Ninth International Heat Transfer Conference, Jerusalem, 1990, pp. 105–110.
[10] S.J. Baldwin, P.R.S. White, A.J. Al-Daini, C.J. Davenport. Investigation of the gas side flow field in multilouvred ducts with flow reversal. Proceedings of the Fifth International Conference on Numerical Methods in Laminar and Turbulent Flow, Montreal, 1987, pp. 482–495.
[11] B.L. Button, R. Tura, C.C. Wright. Investigation of the airflow through louvred rectangular ducts using laser Doppler anemometry. Proceedings of the Second International Symposium on Applications of Laser Doppler Anemometry to Fluid Mechanics, Lisbon, 1984, pp. E2–E5.
[12] M. Hiramatsu, K. Ota. Heat transfer analysis for heat exchanger fins. Paper B303. Proceedings of the Nineteenth National Heat Transfer Symposium of Japan, 1982.
[13] K. Suga, H. Aoki, T. Shinagawa. Numerical analysis on two-dimensional flow and heat transfer of louvered fins using overlaid grids. JSME International Journal, Series 2 33 (1) (1990) 122–127.
[14] K. Suga, H. Aoki. Numerical study on heat transfer and pressure drop in multilouvered fins. Proceedings of the

ASME/JSME Thermal Engineering Joint Conference, Reno, 1991, pp. 361–368.

[15] M. Hiramatsu, T. Ishimaru, K. Matsuzaki. Research on fins for air conditioning heat exchangers (1st Report, Numerical analysis of heat transfer on louvered fins). JSME International Journal, Series II 33 (4) (1990) 749–756.

[16] S. Ikuta, Y. Sasaki, K. Tanaka, M. Takagi, R. Himeno. Numerical analysis of heat transfer around louver assemblies. SAE Paper No. 900081, 1990.

[17] A. Achaichia, M.R. Heikal, Y. Sulaiman, T.A. Cowell. Numerical investigation of flow and friction in louvred fin arrays. Proceedings of the Tenth International Heat Transfer Conference, Brighton, 1994.

[18] M.Y. Ha, K.C. Kim, S.H. Koak, K.H. Kim, K.I. Kim, J.K. Kang, T.Y. Park. Fluid flow and heat transfer characteristics in multi-louvered fin heat exchanger. SAE Paper No. 950115, 1995.

[19] T. Shinagawa, H. Aoki, K. Suga. A study of finned heat exchanger: 5th report, a method for measuring the heat transfer coefficient of the louvers. Proceedings of the Twenty-third National Heat Transfer Symposium of Japan, 1986, pp. 340–342.

[20] S.V. Patankar. Numerical Heat Transfer and Fluid Flow. Hemisphere Publishing Corporation, 1980.

[21] M.A. Leschziner. Practical evaluation of three finite difference schemes for the computation of steady-state recirculating flows. Computer Methods in Applied Mechanics and Engineering 23 (1980) 293–312.

[22] P.G. Huang, B.E. Launder, M.A. Leschziner. Discretization of non-linear convection processes: a broad-range comparison of four schemes. Computer Methods in Applied Mechanics and Engineering 48 (1985) 1–24.

[23] J.P. Van Doormal, G.D. Raithby. Enhancements of the SIMPLE method for predicting incompressible fluid flows. Numerical Heat Transfer 7 (1984) 147–163.

[24] W.M. Kays, A.L. London. Compact Heat Exchangers, McGraw-Hill, New York, 1984.

[25] A.A. Antoniou. Measurements of local heat transfer, velocity and turbulence intensity values in louvred arrays. PhD thesis. CNAA, Brighton Polytechnic, 1989.